

PAPER • OPEN ACCESS

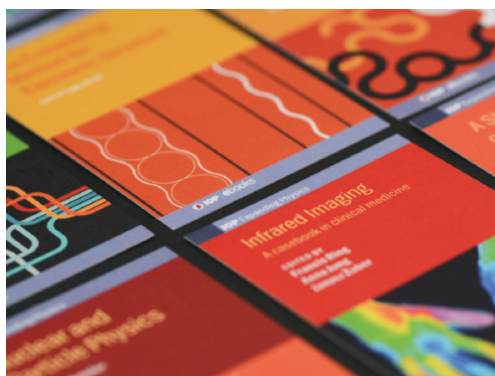
The microwave properties of tin sulfide thin films prepared by RF magnetron sputtering techniques

To cite this article: Mircea Dragoman *et al* 2022 *Nanotechnology* **33** 235705

View the [article online](#) for updates and enhancements.

You may also like

- [Microwave-Assisted Synthesis of Tin Sulfide/Reduced Graphene Oxide Nanocomposites As Anode Material for High-Performance Lithium-Ion Batteries](#)
Jeng-Yu Lin and Hsin-Ping Ho
- [Electronic Structure and Redox Behavior of Tin Sulfide Films Potentiostatically Formed on Tin](#)
Jozefina Kati, Mirjana Metikoš-Hukovi, Iva Šari et al.
- [Structural and optical properties of tin \(II\) sulfide thin films deposited using organophosphorus precursor \(Ph₃PS\)](#)
Kawther Assili, Khaled Alouani and Xavier Vilanova



IOP | ebooks™

Bringing together innovative digital publishing with leading authors from the global scientific community.

Start exploring the collection—download the first chapter of every title for free.

The microwave properties of tin sulfide thin films prepared by RF magnetron sputtering techniques

Mircea Dragoman¹ , Martino Aldrigo¹ , Adrian Dinescu¹ ,
Sergiu Iordanescu¹ , Cosmin Romanitan¹ , Silviu Vulpe¹ ,
Daniela Dragoman^{2,3} , Tudor Braniste⁴ , Victor Suman⁵,
Emil Rusu⁵  and Ion Tiginyanu⁶ 

¹ National Institute for Research and Development in Microtechnologies, 126A Erou Iancu Nicolae Street, 077190 Voluntari (Ilfov), Romania

² Univ. of Bucharest, Physics Faculty, PO Box MG-11, 077125 Bucharest, Romania

³ Academy of Romanian Scientists, Str. Ilfov 3, 050044 Bucharest, Romania

⁴ National Center for Materials Study and Testing, Technical University of Moldova, 168 Stefan cel Mare Av., 2004 Chisinau, Moldova

⁵ Institute of Electronic Engineering and Nanotechnologies, Academiei Street 3/3, 2028 Chisinau, Moldova

⁶ Academy of Sciences of Moldova, 1 Stefan cel Mare Av., 2004 Chisinau, Moldova

E-mail: martino.aldrigo@imt.ro

Received 1 November 2021, revised 21 January 2022

Accepted for publication 2 March 2022

Published 17 March 2022



Abstract

In this paper we present the microwave properties of tin sulfide (SnS) thin films with the thickness of just 10 nm, grown by RF magnetron sputtering techniques on a 4 inch silicon dioxide/high-resistivity silicon wafer. In this respect, interdigitated capacitors in coplanar waveguide technology were fabricated directly on the SnS film to be used as both phase shifters and detectors, depending on the ferroelectric or semiconductor behaviour of the SnS material. The ferroelectricity of the semiconducting thin layer manifests itself in a strong dependence of the electrical permittivity on the applied DC bias voltage, which induces a phase shift of 30 degrees mm^{-1} at 1 GHz and of 8 degrees mm^{-1} at 10 GHz, whereas the transmission losses are less than 2 dB in the frequency range 2–20 GHz. We have also investigated the microwave detection properties of SnS, obtaining at 1 GHz a voltage responsivity of about 30 mV mW^{-1} in the unbiased case and with an input power level of only 16 μW .

Keywords: ferroelectrics, microwaves, semiconductors, thin films, tin sulfide, detector, phase shifter

(Some figures may appear in colour only in the online journal)

1. Introduction

Tin sulfide (SnS) is a direct bandgap semiconductor (bandgap $E_g = 1.3 \text{ eV}$), and a nontoxic and earth-abundant material used in many photonic and electronic applications, such as

photodetectors, solar cells, photochemical cells, battery anodes, and gas sensors [1, 2]. Due to its physical properties and especially ferroelectricity, SnS is nowadays one of the most studied two-dimensional (2D) compounds, since it is a van der Waals material formed by several piled up monolayers [3]. SnS films with a few-atom thickness have found applications in ferroelectric analogue synaptic devices for artificial neural network applications [4] and nonlinear optics [5]. However, the microwave properties of 2D SnS are completely unknown, as well as the ones of other 2D



Original content from this work may be used under the terms of the Creative Commons Attribution 4.0 licence. Any further distribution of this work must maintain attribution to the author(s) and the title of the work, journal citation and DOI.

ferroelectrics. Up to now, the applications of 2D ferroelectrics are related to switchable rectification, field-effect transistors with memory, and ferroelectric tunneling diodes [6]. AlScN is the single semiconducting ferroelectric [7] that has applications in microwaves at the wafer scale, especially in surface acoustic wave resonators [8] and Lamb resonators (in this case, by exploiting its parent material ScAlN) [9].

We have shown recently that HfO₂-based ferroelectrics having a similar few-nanometer thickness have important applications in microwaves such as phased arrays [10], since the electrical permittivity ϵ_r is considerably tuned at few Volts of applied DC bias voltages, in deep contrast with perovskite ferroelectrics where tens if not hundreds of Volts are necessary to significantly change ϵ_r . For all the previous reasons, the role of this work is to extend our previous research to the microwave applications of semiconducting ferroelectric SnS, which can be easily grown on silicon dioxide/silicon (SiO₂/Si) wafers.

2. Materials and methods

The SnS films with the thickness of 10 nm were deposited in standard water-cooled RF magnetron, powered at 13.6 MHz. The target used for the deposition process was fabricated in-house by pressing SnS microcrystals. The SnS crystals were synthesized using Bridgman method at the Institute of Electronic Engineering and Nanotechnology. The high purity of the bulk crystalline SnS resulted from the 5 N purity of Sn and S initial components purchased from Merck Company. For the target preparation, the synthesized SnS crystals were crumbled to small pieces, followed by sieving of the resulted crystallites using a mesh with holes of 100 μm . The fraction of crystallites with the diameter less than 100 μm was further used for target preparation under uniaxial pressure of 200 kg cm⁻² in a crucible with a diameter of 50 mm. The RF deposition occurred at a magnetron power of 80 W in 50 ml min⁻¹ Ar flow, whereas the pressure in the working chamber was 7.4 mBa. The rotating substrate was positioned at 80 mm in front of the target and was heated at 200 °C. The thickness of the film was measured during the deposition process using a quartz sensor with standardized coefficient from Tectra GmbH Thickness Monitor that allows measurements of film thicknesses as low as 0.1 nm.

To obtain information about the structural and compositional properties of the tin sulfide layer, x-ray reflectivity (XRR) measurements were performed on a Rigaku SmartLab diffractometer employing CuK α_1 radiation with wavelength of 0.154 06 nm. Reflectivity curves were measured in the range of the incidence angle $\theta_i = 0\text{--}5^\circ$ with a step width of 0.001° and a scan rate equal to 0.2° min⁻¹ using a high-resolution setup with a divergent height limiting slit equal to 5 mm. The incident and receiving slits were fixed to 0.2 mm. The grazing incidence x-ray diffraction pattern is shown in figure 1.

The broad diffraction features were interpreted as overlapped diffraction peaks assigned as (012), (102), (110), (006), (115), and (106) reflections of orthorhombic SnS with the following lattice parameters: $a = 0.39$ nm, $b = 0.43$ nm, and $c = 1.12$ nm. The indexing was performed using ICDD (International Crystallography for Diffraction Data) database

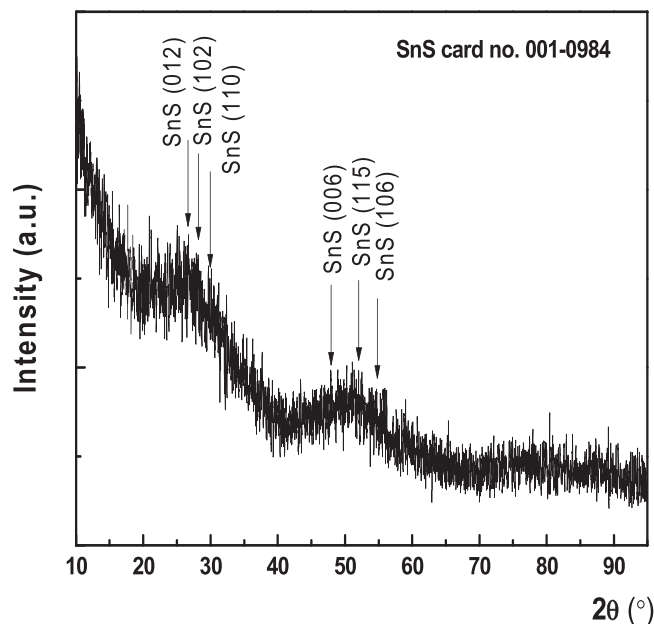


Figure 1. GI-XRD pattern at incidence angle of 0.5°. Diffraction features were identified as overlapped reflections of SnS.

with card no. 001-0984. The results indicate that the SnS thin film has a disordered nano crystalline-like structure, resulted from the relatively low temperature of the substrate (200 °C) during the RF deposition process. The SnS stoichiometry was confirmed by energy dispersive x-ray (EDX) measurements with Vega TS 5130 Electron Microscope.

The SnS thin film was deposited on SiO₂ (with thickness of 50 nm) thermally grown on a 4 inch wafer of high-resistivity silicon (HRSi, Float-Zone Hyper Pure Silicon (FZ-HPS) P(100) by Topsil, resistivity $\rho > 10000$ Ω cm), with thickness of 525 μm . The wafer was cut in samples; one of these samples is shown in figure 2(a): it contains (i) structures with two metal contacts for DC characterization and (ii) other structures for microwave characterization. Each microwave structure is a coplanar waveguide line (CPWs, with a total length of 500 μm), in the center of which an interdigitated capacitor (IDC) is embedded (see figure 2(b)). The SEM images in figure 2(c) show the details of IDC's digits. The metallization of the CPW loaded with the IDC was made by electron beam (e-beam) deposition (Ti/Au, thickness of 10 nm/90 nm, where the Ti film served as adhesion layer). Each IDC is formed by 250 digits and each digit has a width of 250 nm, whereas the gap between two adjacent digits is 200 nm. The total length of each IDC is 100 μm . The IDC is embedded into a CPW line with gap and signal dimensions of 60 μm and 100 μm , respectively, to provide on-wafer measurements with characteristic impedance equal to 50 Ω (standard reference impedance for microwave devices and components).

The specifically designed microwave structure allows applying a horizontal (i.e. in-plane) external electric field E_{ext} between two adjacent digits of the IDCs with opposite polarizations. This way, it is possible to bias the semiconducting ferroelectric SnS thin film, as the ferroelectricity in SnS can be observed only when E_{ext} is parallel with the plane of the film itself [3], in contrast with most other ferroelectrics where the

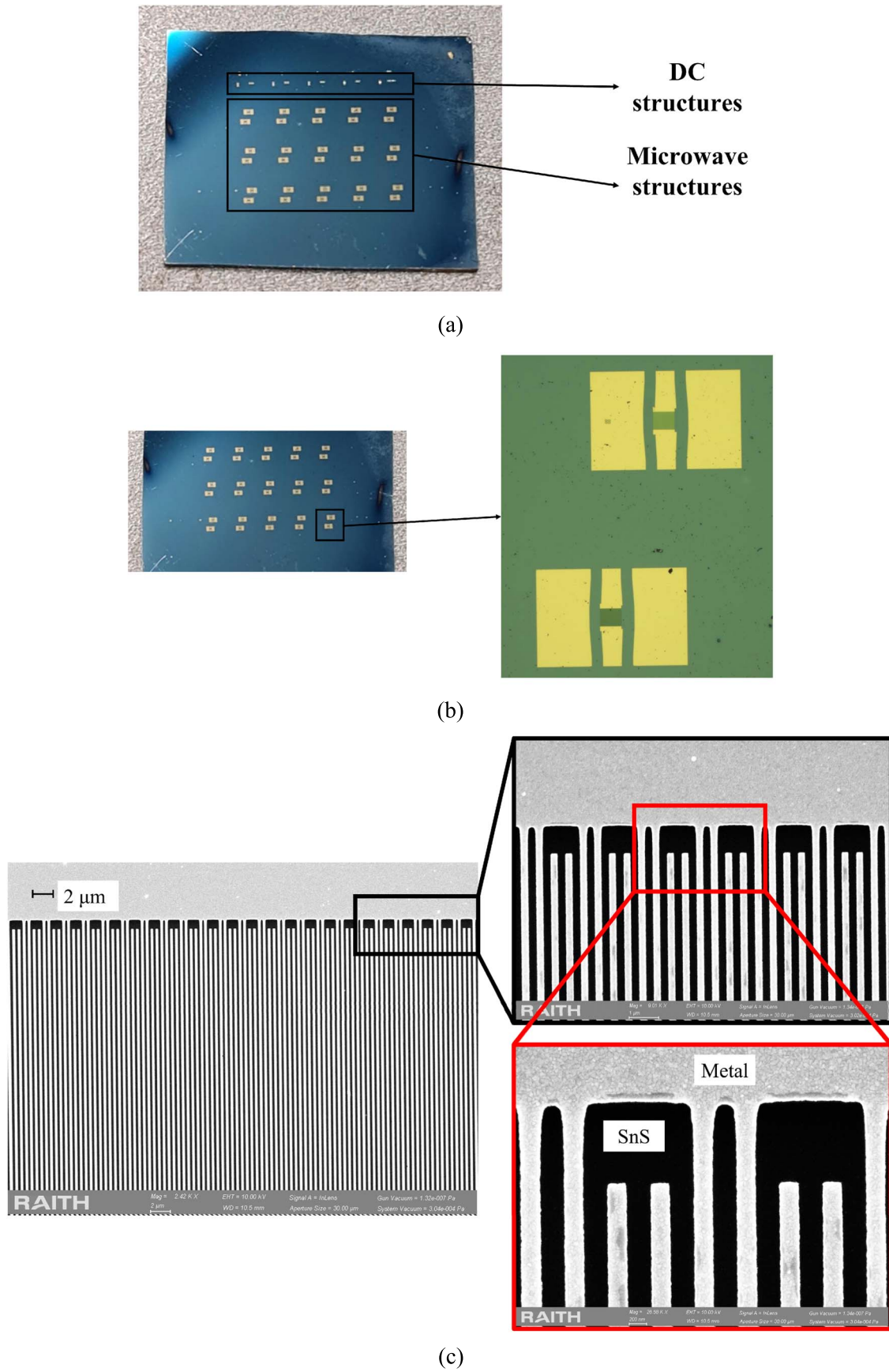


Figure 2. (a) Samples with structures for DC and microwave testing; (b) details of the microwave structures; (c) SEM images of a region of the IDC.

external polarization is out-of-plane. The necessity of an in-plane electrical polarization creates difficulties to demonstrate the ferroelectricity in SnS when DC and low-frequency AC measurements are made [3]. Thus, piezo-force microscopy (PFM) can be made only on corrugated surfaces and the atomic-force microscopy (AFM) tip should not be perfectly perpendicular to the thin film surface to be able to collect small amounts of the polarization signal; more details about PFM and AFM measurements performed on few-layer SnS can be found in [11]. For all these reasons, the polarization-electric field $P(E)$ curve cannot be measured directly, as it could give rise to misinterpretations. However, another way to observe the ferroelectricity from a DC characterization is the current–voltage (I – V) dependence, which was measured for SnS thicknesses ranging from one monolayer (0.6 nm) up to 20 nm, thus evidencing the hysteretic nature of the material. After integration of the DC current, a broken $P(E)$ curve was obtained with a coercive field of just 10.7 kV cm^{-1} [11], whereas in other publications it was around 50 – 60 kV cm^{-1} [4], and the remanent polarization value also varies significantly from report to report. These scattered results could be ascribed to the fact that SnS thin films were grown by different methods on different substrates and mainly due to the strong influence of the conductivity on the measurement of $P(E)$, which deteriorates and even destroys the ferroelectric properties when they are investigated under a strong DC field. We know that the I – V dependence of a ferroelectric with vertical polarization represents the leakage current of a metal–ferroelectric–metal (MFM) capacitor, whereas in the case of in-plane polarization ferroelectrics (like SnS) the I – V curve originates from the superposition of many horizontal current flows and from the current induced by charges trapped in the surface defects, these charges being released when the applied DC field is exceeding a specific built-in field. Thus, the effect of the high conductivity of the SnS as semiconductor is to diminish or even damage its ferroelectric features; hence, the polarization curves appear broken and not saturated in DC regime, as demonstrated in [12] for a conductive BiFeO_3 ceramic, whose hysteresis loops exhibit a gap between the starting and ending applied fields. In fact, the charge Q associated to the polarization switching depends (in general) on the remanent polarization P_r , the capacitor area A , the electrical conductivity σ of the ferroelectric under test, E_{ext} , and the measuring time t , as follows [12, 13]:

$$Q = 2P_r A + \sigma E_{ext} A t. \quad (1)$$

Equation (1) states clearly that, for large values of σ (typically greater than 10^{-6} S m^{-1}), the polarization contributed by domain switching is hidden by the conductivity of the ferroelectric material. At the same time, the relative permittivity is $\varepsilon_r = \varepsilon' + j\varepsilon'' = \varepsilon' + j\sigma/(\omega\varepsilon_0)$, where ω is the angular frequency. Hence, we can expect that within a certain voltage range $[-V_{th}, V_{th}]$ (where V_{th} is a threshold DC bias voltage) we have $\sigma \ll 10^{-6} \text{ S m}^{-1}$ and $\varepsilon_r \approx \varepsilon' = \varepsilon'(V_b)$ (V_b is the bias voltage), meaning that the ferroelectric behaviour is prevalent. An increase of σ entails that $\varepsilon_r \approx j\varepsilon'' = j\sigma/(\omega\varepsilon_0)$ or, in other words, the dependence of ε_r on V_b vanishes, since the conduction mechanism becomes dominant and the device acts like a semiconductor diode that rectifies the AC signal.

3. Results and discussion

From the previous sections, it is clear that new methods need to be found to deal with the in-plane ferroelectricity of SnS thin films; therefore, we have chosen the microwave characterization. In this respect, the measurements of the CPW loaded with the IDC were performed using a vector network analyzer (VNA, Anritsu 37397D), together with a standard short-open-load-thru (SOLT) calibration kit (see [14] and references herein for more details). The VNA was connected to a DC source (Agilent E3631A) for the DC biasing of the microwave structures. We carried out the high-frequency measurements (see [15] and references herein for a comprehensive review about microwave measurements of nanoscale ferroelectric-based devices and components) on many structures of the type shown in figures 2(b), (c), by applying a DC polarity to each electrode of the CPW line (more in detail, the two polarities were equal in amplitude but opposite in sign), then we reversed the polarity to double check the measured scattering (S) parameters and observe any difference. All the IDCs under test exhibited a constant electrical behaviour (in terms of S -parameters); this represents an indirect proof of the homogeneity of the deposited SnS thin film. The outcome of this comparison was that no significant change in the reflection (S_{11}) and transmission (S_{12}) coefficients could be observed when the DC bias polarity was reversed, these results being depicted in figure 3. Figures 3(a) and (b) give the evidence (in terms of $|S_{11}|$) that the CPW with the IDC is well matched to the characteristic impedance of 50Ω for increasing frequencies, and that the SnS-based CPW structure is essentially a capacitor over the entire band 0 – 20 GHz . $|S_{12}|$ is represented in figure 3(c) and shows transmission losses around 1 dB from 3.6 GHz (at 0 V) and 5.3 GHz (at 5 V) up to 20 GHz or, in other words, the unique ferroelectric signature of SnS improves significantly the high-frequency transmission with respect to other oxide ferroelectrics with larger loss tangent values. A possible explanation is that the SnS thin film involved, representing a nanocrystalline semiconductor material with a large bandgap, has a reduced number of shallow defects at the energy levels in microwaves, which are many orders of magnitude smaller than that of the bandgap energy [16]. Thus, the SnS thin film is nearly transparent at microwave frequencies.

Figure 4(a) displays the total phase shift as it was extracted by the measured phase of the transmission parameter S_{12} : we see that at 1 GHz we have a total phase shift of about $30 \text{ degrees mm}^{-1}$ for a polarization of $\pm 5 \text{ V}$ at the two ports of the CPW line, then it decreases smoothly to $8 \text{ degrees mm}^{-1}$ at 10 GHz . This is the direct evidence that the SnS is ferroelectric, since the phase of S_{12} depends on the applied DC bias voltage [17]. Figure 4(a) also proves that only slight differences occur when reversing the polarization sign between the two ports. A further proof of this fact is the dependence of the effective permittivity ε_{eff} on the DC bias (figure 4(b)), as it happens in any ferroelectric. To obtain the curves in figure 4(b) (never reported before for SnS), we used the conformal mapping method (CMM) to derive the capacitance/effective permittivity of the IDC/multi-layer substrate (respectively), starting from the following assumptions/considerations: (i) the capacitance

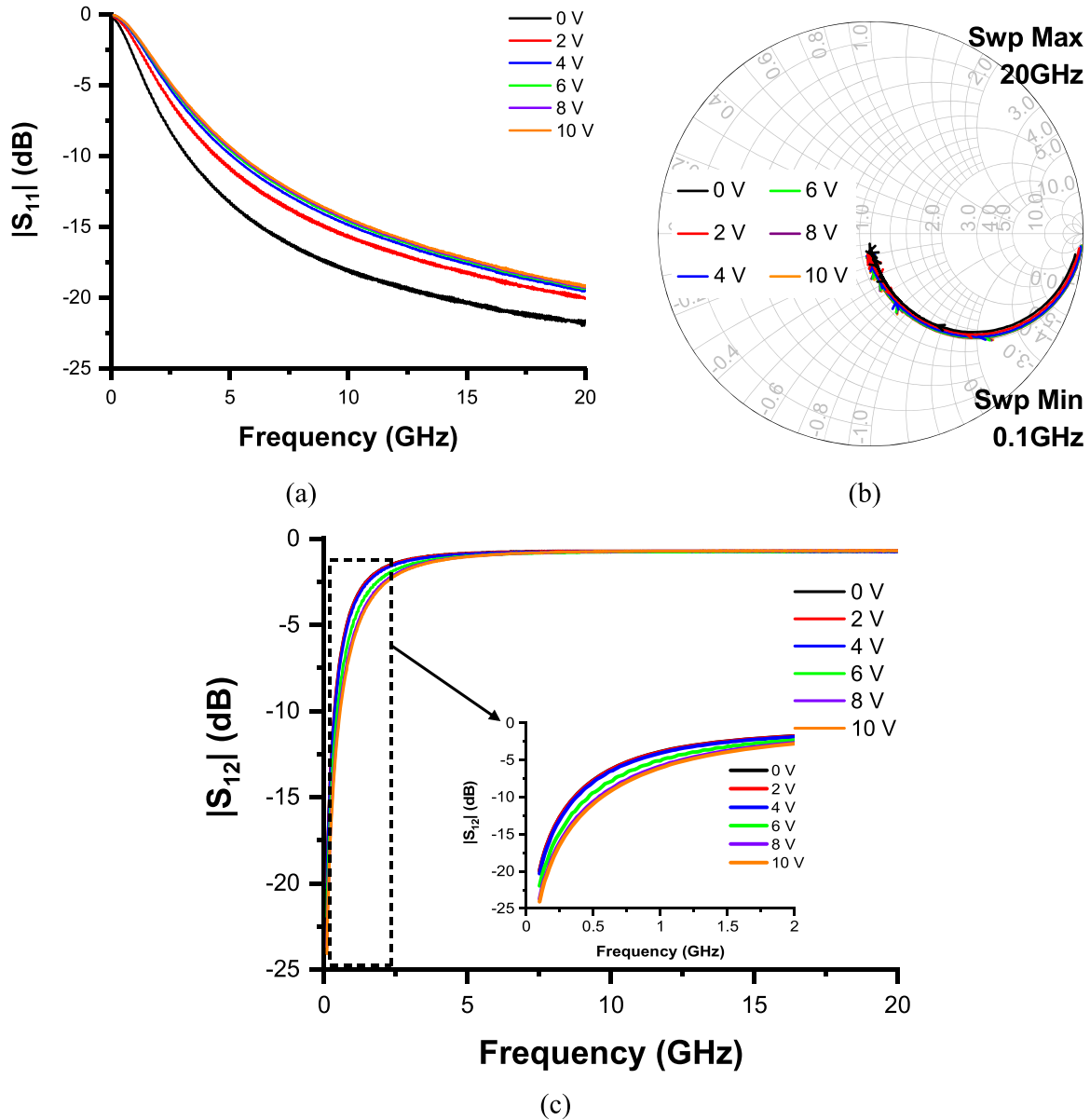


Figure 3. (a) $|S_{11}|$ dependence on the frequency and applied DC voltage; (b) Smith chart of $|S_{11}|$ dependence on the frequency and applied DC voltage; (c) $|S_{12}|$ dependence on the frequency and applied DC voltage (inset: magnification in the band 0–2 GHz).

of the IDC is mainly due to an equivalent series capacitor, which in turn depends on the electric field applied in-between the digits; (ii) SnS has a nominal $\epsilon_r = 12$ at 0 V bias, which is very close to that of silicon; hence, one can expect that ϵ_{eff} at 0 V is the same as that of an IDC on pure silicon; (iii) the measured capacitance of the IDC decreases with the applied bias; hence, a decrease of the effective permittivity is expected as well [18]. We stress here that the extraction of the relative permittivity from such multilayer structures based on IDCs on ultra-thin layers is not a trivial issue. Moreover, for many applications of interest in the microwave range, ϵ_{eff} is much more useful, as at high frequencies the significance of ϵ_r must be replaced with ϵ_{eff} . ϵ_{eff} depends strongly on ϵ_r but, especially in open guiding structures like microstrip or CPW lines (largely exploited in microwaves), ϵ_{eff} is much more significant as it also considers the line geometry, i.e. both reflection and

transmission of the electromagnetic field in the propagating structure [18, 19]. The results shown in figure 4 also prove that the phase shift and the change in the effective permittivity are solely due to the SnS thin film, and not intrinsic to the presented device geometry, nor due to polarization effects in the Si support wafer, since the latter is of the high-resistivity type with a SiO₂ passivation layer interposed between the Si and the SnS. Hence, there is no reason to attribute the observed macroscopic ferroelectric effect to the SiO₂/Si substrate. Figure 4(b) also reveals an important property of SnS thin films: when increasing the externally applied electric field (via a DC bias voltage), a saturation of the polarizable charges occurs in AC regime, which results in a progressive decrease of ϵ_{eff} for increasing bias values until ϵ_{eff} reaches a plateau (between 4 and 5). In other words, beyond ± 4 V (which represents the threshold bias voltage V_{th} mentioned previously) the behaviour

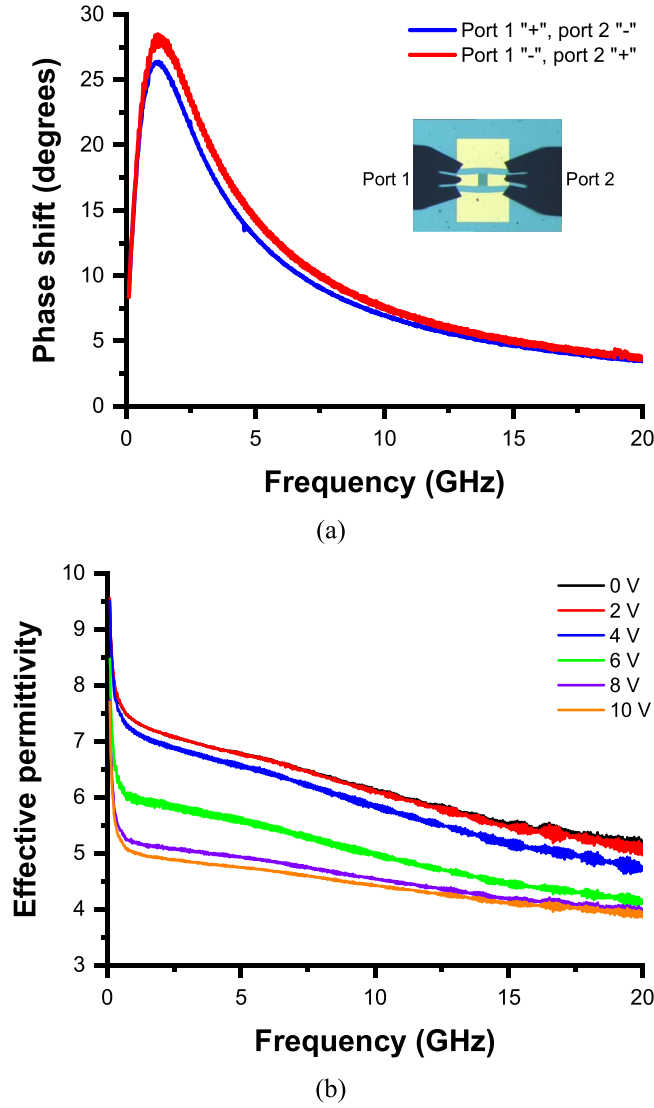


Figure 4. (a) Total phase shift as a function of frequency; (b) effective permittivity of the SnS thin film at microwaves for different bias values.

becomes predominantly of the semiconductor type and ϵ_{eff} does not depend on the applied bias anymore. Furthermore, the SnS has a noticeably high electric breakdown, since applied DC bias voltages of ± 8 V do not have any macroscopic effect on the electrical properties.

In [11] the authors measured a coercive voltage (i.e. the minimum voltage at which the ferroelectric switches) of 4.3 V for few-layer SnS samples with the thickness of 1–2 nm. In our case, we observed that beyond 10 V the effective permittivity no longer changes, thus indicating that the coercive field has been already reached.

We also performed DC measurements of the same SnS CPW structures to verify if the microwave response originates from a ferroelectric IDC or there is a Schottky junction at the metal/SnS interface. In this respect, we used a Keithley SCS 4200 station, where the probe station for on-chip measurements is located inside a Faraday cage, and its channels are connected to the station via low-noise amplifiers. The experimental I – V dependence is displayed in figure 5(a). We know that Ti/Au is a

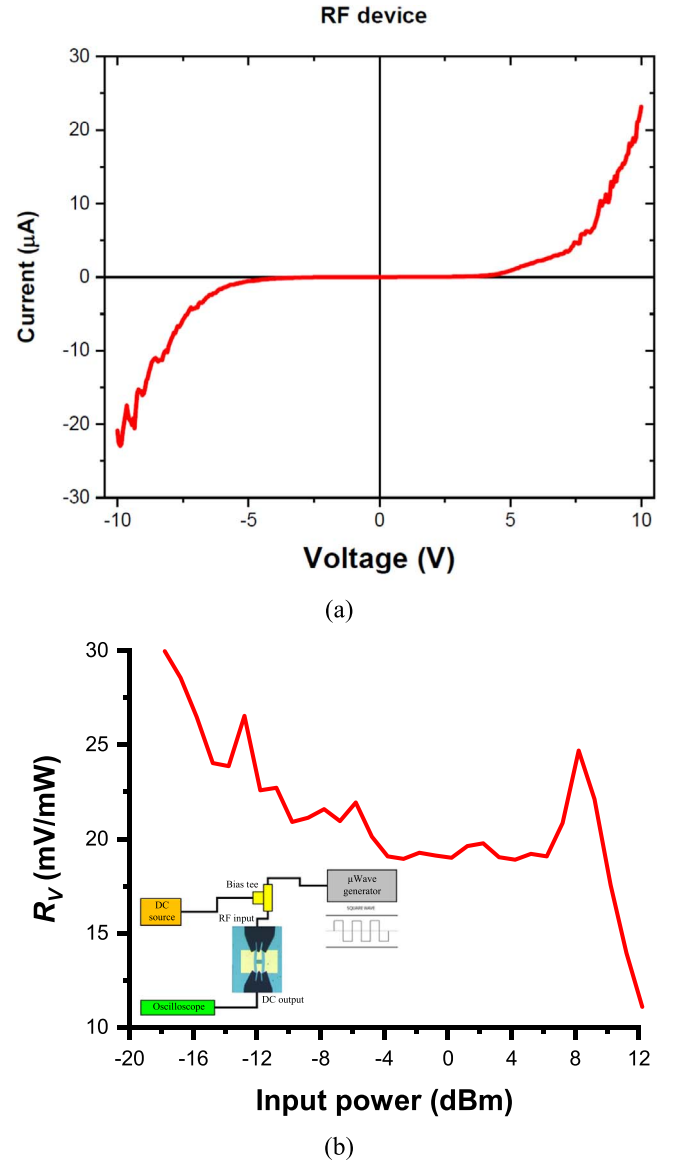


Figure 5. (a) Measured DC I – V dependence; (b) voltage responsivity R_V as a function of the input power at 1 GHz (inset: RF detection setup).

resistive contact for SnS [20], since titanium has a work function comparable to that of SnS. As one can see from figure 5(a), in the range $[-5, +5]$ V the SnS thin film has a very low DC conductivity (the average current in the mentioned voltage range is just 5 nA), which means that the results obtained at microwaves reflect the ferroelectric, not semiconducting, nature of the SnS thin film, as it will be detailed in the following.

Finally, we prepared the setup displayed in the inset of figure 5(b) to verify the microwave detection properties of SnS, which presently are unknown. The microwave generator was used to provide a square wave modulating signal (with modulation frequency of 100 Hz) to a sinusoidal RF carrier in the band 0.9–3.5 GHz. The dependence at 1 GHz of the voltage responsivity R_V on the input microwave power is represented in figure 5(b) for the case of 0 V bias. This frequency was chosen as the one providing the highest R_V in the considered frequency range. It must not surprise that 1 GHz is

also the frequency at which the phase shift in figure 4(a) is maximum. In fact, as demonstrated in [21], an increased AC conduction of the ferroelectric domain walls in the gigahertz range occurs in nanometric scale ferroelectrics, which is likely due to morphological roughening of the walls and local charges induced by the SnS disordered nano crystalline-like structure. In other words, this gigahertz conduction manifests in a twofold way: (i) maximization of microwave phase shift; (ii) maximization of microwave detection. One can notice that the responsivity is very good, considering that the research on SnS is still in its infancy and no SnS-based microwave devices exist so far to demonstrate its high-frequency capabilities, meaning that no comparison can be made with standard Schottky detectors. In detail, R_V is equal to about 30 mV mW^{-1} for an input power of -18 dBm (i.e. $16 \mu\text{W}$), whereas between -6 dBm and 6 dBm (i.e. between 0.25 and 4 mW) it keeps an average value of 20 mV mW^{-1} , finally decreasing to about 12 mV mW^{-1} at an input power of 12 dBm (i.e. 16 mW) after an abrupt increase for an input power of 8 dBm (i.e. 6.31 mW) probably due to nonlinear phenomena inside the SnS thin film (which induce different RF-to-DC power conversion efficiencies). The chosen range of input microwave power represents the minimum (i.e. -18 dBm) and maximum (i.e. 12 dBm) power that can be detected by the SnS layer beyond the noise level and avoiding distortion phenomena due to intermodulation effects.

4. Conclusion

In this paper, we have presented the microwave properties and performance of a thin film of tin sulfide (SnS) grown on a silicon dioxide/silicon wafer by RF magnetron sputtering. In detail, we have shown that a coplanar waveguide line with an embedded interdigitated capacitor deposited on the tin sulfide layer acts as a ferroelectric device with in-plane polarization and low transmission losses in the frequency range $2\text{--}20 \text{ GHz}$. Even if the extraction of the dielectric constant from such multilayer structures on nanoscale films is not a trivial issue, we have obtained the effective permittivity and the phase shift on a large frequency range and as a function of the applied DC bias voltage. A big advantage is represented by the fact that the total phase shift can be engineered at any desired value by using multiple interdigitated capacitors connected in series and/or parallel configuration, since the microwave losses are less than 1 dB all over the band of interest. This aspect, together with the possibility of depositing the SnS thin films directly on silicon dioxide/silicon substrates, offers promising perspectives of exploiting such nanoscale semiconducting ferroelectrics into future nanoelectronics for high-frequency applications.

Acknowledgments





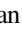





This research was partially funded by the European Commission under the Grant No. 951761 ‘NANO-EH’ and under the Grant No. 810652 ‘NanoMedTwin’, by the Romanian Ministry of

Research, Innovation and Digitalization: CCCDI-UEFISCDI project PN-III-P4-ID-PCCF-2016-0033, within PNCDI III, and by the National Agency for Research and Development of the Republic of Moldova under the Grant No. 20.80009.50007.20 and the Grant No. 20.80009.50007.02.

Data availability statement

The data that support the findings of this study are available upon reasonable request from the authors.

ORCID iDs

Mircea Dragoman  <https://orcid.org/0000-0001-6886-5295>
 Martino Aldrigo  <https://orcid.org/0000-0003-2257-1966>
 Adrian Dinescu  <https://orcid.org/0000-0002-6216-2035>
 Sergiu Iordanescu  <https://orcid.org/0000-0001-9471-6306>
 Cosmin Romanitan  <https://orcid.org/0000-0002-5615-6624>
 Silviu Vulpe  <https://orcid.org/0000-0002-3269-1382>
 Daniela Dragoman  <https://orcid.org/0000-0003-4241-0000>
 Tudor Braniste  <https://orcid.org/0000-0001-6043-4642>
 Emil Rusu  <https://orcid.org/0000-0001-9010-4927>
 Ion Tiginyanu  <https://orcid.org/0000-0003-0893-0854>

References

- [1] Koteeswara Reddy N, Devika M and Gopal E S R 2015 *Crit. Rev. Solid State Mater. Sci.* **40** 359
- [2] Norton K J, Alam F and Lewis D J 2021 *Appl. Sci.* **11** 2062
- [3] Barazza-Lopez S, Fregoso B M, Villanova J W, Parkin S S P and Chang K 2021 *Rev. Mod. Phys.* **93** 011001
- [4] Kwon K C et al 2020 *ACS Nano* **14** 7628
- [5] Wu L et al 2018 *Adv. Opt. Mater.* **6** 1700985
- [6] Liu M, Liao T, Sun Z, Gu Y and Kou L 2021 *Phys. Chem. Chem. Phys.* **23** 21376
- [7] Fichtner S, Wolff N, Lofink F, Kienle L and Wagner B 2019 *J. Appl. Phys.* **125** 114103
- [8] Wang J, Park M, Mertin S, Pensala T, Ayazi F and Ansari A 2020 *J. Microelectromech. Syst.* **29** 741
- [9] Rassay S, Mo D, Li C, Choudhary N, Forgey C and Tabrizian R 2021 *IEEE Electron. Device Lett.* **42** 1065
- [10] Dragoman M, Modreanu M, Povey I, Iordanescu S, Aldrigo M, Dinescu A, Vasilache D and Romanitan C 2018 *Electron. Lett.* **54** 469
- [11] Bao Y et al 2019 *Nano Lett.* **19** 5109
- [12] Jin L, Li F and Zhang S 2014 *J. Am. Ceram. Soc.* **97** 1
- [13] Dawber M, Rabe K M and Scott J F 2005 *Rev. Mod. Phys.* **77** 1083
- [14] Dragoman M, Modreanu M, Povey I M, Iordanescu S, Aldrigo M, Romanitan C, Vasilache D, Dinescu A and Dragoman D 2017 *Nanotechnology* **28** 38LT04
- [15] Dragoman M, Aldrigo M, Dragoman D, Iordanescu S, Dinescu A and Modreanu M 2021 *Phys. Status Solidi RRL* **15** 2000521
- [16] Kumagai Y, Burton L A, Walsh A and Oba F 2016 *Phys. Rev. Appl.* **6** 014009
- [17] De Flaviis F, Alexopoulos N G and Stafsudd O M 1997 *IEEE Trans. Microw. Theory. Technol.* **45** 963

-
- [18] Wang Z, Liu J and Liu L 2006 *IEEE Trans. Instrum. Meas.* **55** 350
- [19] Yoon Y J and Kim B 2000 *Proc. of IEEE 9th Topical Meeting on Electrical Performance of Electronic Packaging* vol 163
- [20] Nandanapalli K R, Mudusu D and Reddy G K 2019 *Mater. Sci. Semicond. Process.* **100** 192
- [21] Tselev A, Yu P, Cao Y, Dedon L R, Martin L W, Kalinin S V and Maksymovych P 2016 *Nat. Commun.* **7** 1160